Int. J. Electron. Commun. (AEÜ) 96 (2018) 178–183

Contents lists available at ScienceDirect

International Journal of Electronics and Communications (AEÜ)

journal homepage: www.elsevier.com/locate/aeue

Regular paper

Polarization-independent frequency-selective rasorber with a broadened absorption band

Qiang Chen, Min Guo *, Zhanshan Sun, Di Sang, Yunqi Fu

College of Electronic Science, National University of Defense Technology, Changsha 410073, China

ARTICLE INFO

Article history:
Received 25 April 2018
Accepted 8 September 2018

Keywords:
Frequency-selective rasorber
Micro resonator
Transmission
Absorption

ABSTRACT

A polarization-independent frequency selective rasorber (FSR) with a transmission band at high frequency and a broadened absorption band at low frequency is designed and analyzed in this paper. The FSR consists of a resistive sheet and a bandpass frequency selective surface (FSS). A strip-type micro resonator (MR) is developed and applied in the resistive element. The MR is equivalent to a parallel LC circuit and resonates at the transmission band. The induced surface current distributions on the resistive element at different frequencies can be controlled as expected using the MRs, so that a high in-band transmission at high frequency and an absorption band at low frequency can be obtained, which are almost independent to each other. The absorption bandwidth can be broadened by cascading more MRs with several resistor-loaded metallic strips. Besides, due to the tiny dimensions of the MRs, polarization-independent absorptive/transmissive performances can be achieved by printing two orthogonal arrays of resistive elements on different surfaces of a dielectric substrate. The performance of the FSR is verified by both numerical simulation and experimental measurement.

1. Introduction

Frequency-selective surface (FSS) is a kind of periodical structure which has bandpass or bandstop performance [1]. It has been widely applied in radome to reduce radar cross section (RCS) or improve radiation performance of antenna [2]. However, the FSS-based radome can only reduce the monostatic RCS by reflecting the incident wave to other directions, which may be detected by bi-/multi-static radar system. Circuit analog absorber (CAA) is another kind of periodical structure which is usually accomplished by placing resistive sheets upon a conductor-backed substrate spacer. CAA with wideband and polarization-independent absorptive performance has great potential in stealthy technology [3–5], but it cannot be applied in radome to reduce the RCS of antenna directly due to its lossy property.

Based on the theories and designs of FSS and CAA, frequency selective rasorber (FSR, "rasorber" is the combination of the word "radome" and "absorber") is of greater prospect in design of low-observable radome [6]. FSR usually consists of a resistive sheet and a metallic bandpass FSS. FSR performs as a radome at some frequencies (transmission band), where the operating wave can be transmitted with low insertion loss; FSR absorbs the incident wave at the out-of-band frequencies (absorption band), similar to a CAA.

Generally, FSR can be sorted into three kinds based on the relative locations of the transmission band and the absorption band. The first kind of FSR has a transmission band below its absorption band, which has been deeply studied in previous works [7–11] and is relatively easier to design. The second and the third kinds are FSRs with a transmission band above [12–15] or within [16–21] the absorption band. Because traditional resistive sheets by lossy film or loading lumped resistors are usually of high insertion loss at the frequency above the absorption band, it is more difficult to design a resistive sheet which has a transparent window at high frequency.

In practical application, a well-designed FSR radome is usually required to have a polarization-independent and wide absorption band, and a transmission band with low insertion loss. In this paper, we propose a method to broaden the absorption band of FSR to lower frequency and meanwhile maintain a transparent window at high frequency. Its resistive sheet is realized by inserting several micro resonators (MR) into a resistor-loaded linear metallic dipole. The MR is a tiny strip-type parallel LC structure, which is designed to resonate at the transmission band, so to control the induced surface current distribution on the resistive sheet at different frequencies and realize a transparent window at high frequency. The absorption bandwidth is broadened by cascading

* Corresponding author.
E-mail address: guomin14@nudt.edu.cn (M. Guo).

https://doi.org/10.1016/j.aeue.2018.09.013
1434-8411/

three resistor-loaded metallic strips with two MR structures. Polarization-independent absorptive/transmissive performance is achieved by printing two orthogonal linear resistive elements on different surfaces of a dielectric substrate.

2. Single-polarized FSR based on MR

2.1. Analysis of MR

Firstly, we consider a metallic dipole exposed to an incident plane wave. The direction of E-field is parallel with the dipole. The relationship between the reflection/transmission coefficient and the electrical length l/λ (l is the physical length of the dipole; λ is the free-space wavelength) is analyzed by full-wave simulation software CST. The result is shown in Fig. 1. It is seen that when the electrical length is less than 0.3, the dipole FSS is almost transparent with unity transmission. As the electrical length increases to 0.5, the dipole resonates to be total-reflected.

A linear metallic dipole with length of $l \approx 0.5\lambda_l$ resonates at the frequency f_l. Absorption can be achieved by loading lumped resistor into the dipole element. To obtain a transparent window at a high frequency f_h ($f_h > f_l$), the length of the dipole element should be less than $0.3\lambda_h$. It seems that the dipole element should have a paradoxical dimension. To solve this problem, a MR structure resonating at f_h is introduced into the dipole element.

Fig. 2 shows the simulated frequency response of a metallic dipole element with a MR in the center, and the imaginary part of its equivalent impedance. The thickness and the relative permittivity of dielectric substrate supporting this element is 0.25 mm and $\varepsilon_r = 2.65$. The MR is equivalent to a parallel LC circuit, where the inductor is realized by a meander strip and the capacitor by parallel strips. The MR is designed to resonate at $f_h = 10$ GHz by properly selecting the geometrical parameters. The length of the two short sections around the MR is 7.5 mm, about $\lambda_h/4$ at f_h.

There are two resonance modes of the MR-based dipole element: a parallel resonance and a series resonance. At the parallel resonance frequency of $f_h = 10$ GHz, the imaginary part of the equivalent impedance resonates to be infinite, so that no induced current flows through the MR structure and the whole element is separated to be two short sections in the view of current. Since the length of the short sections is less than $0.3\lambda_h$, the incident wave at f_h can be transmitted with low insertion loss. At the series resonance frequency of $f_l = 6.8$ GHz, the imaginary part of the equivalent impedance resonates to be zero and the MR structure exhibits finite inductive. The whole element resonates to be total-reflected.

A resistive element can be constructed by loading two lumped resistors into the two short sections. The induced surface current

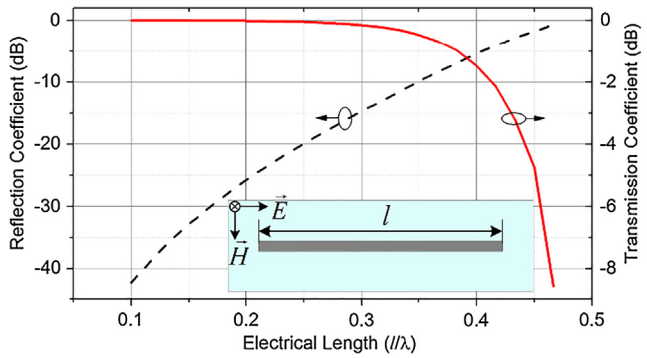

Fig. 1. Reflection/transmission coefficient of a metallic dipole varies with its electrical length.

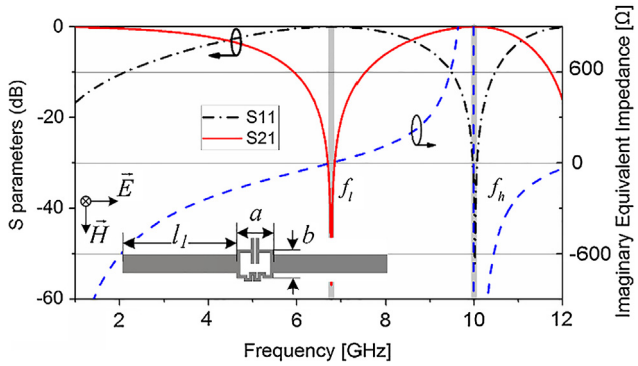

Fig. 2. Dipole element with MR and its frequency response under normal incidence (physical dimensions: $l_1 = 7.5$ mm, $a = 1.9$ mm, $b = 2.4$ mm).

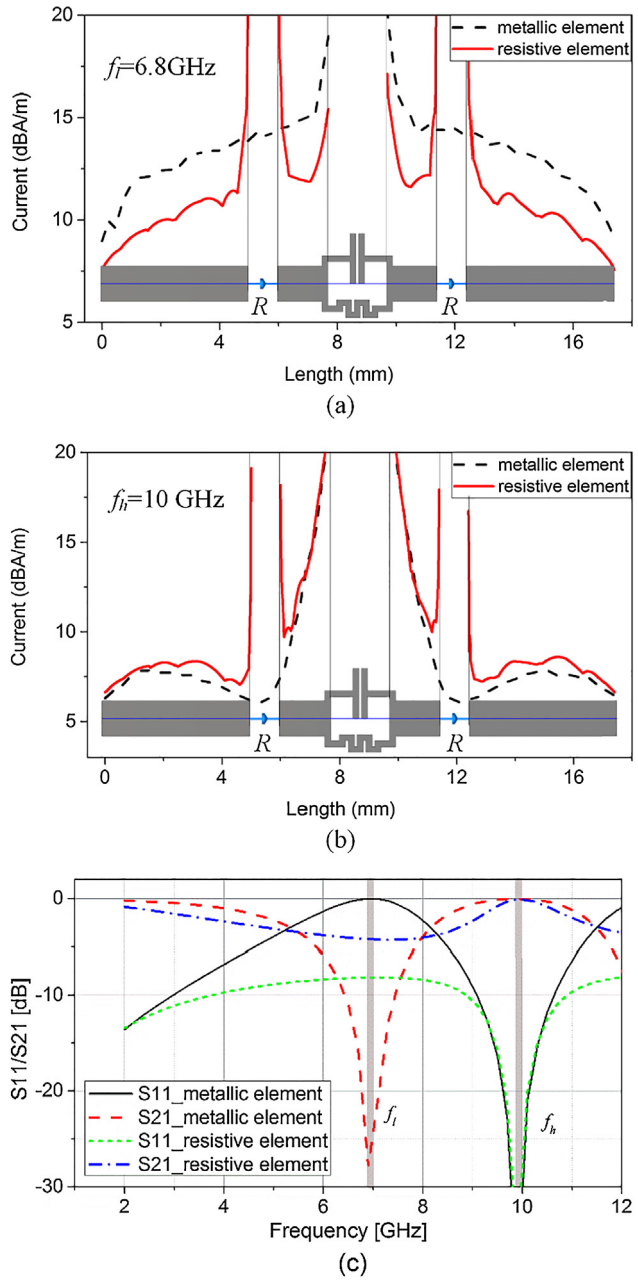

Fig. 3. Surface current distributions on the central line of the metallic element and the resistive element at (a) $f_l = 6.8$ GHz; (b) $f_h = 10$ GHz. (c) The reflection/transmission coefficients of the two FSS elements. The lumped resistor is 150 Ω.

distributions on the original dipole element and the resistive element are analyzed by CST at both the two resonance modes. The current distributions on the central lines of these two elements are compared in Fig. 3(a) and (b). It can be seen that after inserting the lumped resistors, the surface current over the whole element at the first resonance mode (6.8 GHz) is greatly reduced due to the ohm loss, whereas it almost keeps unchanged at the second resonance mode (10 GHz). The incident wave is absorbed at low frequency while transmitted at 10 GHz. Fig. 3(c) gives the simulated reflection/transmission coefficients of FSS by the metallic and the resistive element. It can be seen that both the two FSS elements are nearly transparent at 10 GHz, while the reflection of the resistive element is greatly reduced due to the ohm loss of the lumped resistors.

2.2. Single-polarized FSR with broadband absorption

The resistive element depicted in Fig. 3 has been used to design a single-polarized FSR with absorption at low frequency and transmission at high frequency in [15], but its absorption bandwidth is not broad enough. Theoretically, the larger is the dimension of resistive element, the lower is its resonance frequency, but lengthening the dimension of resistive element will result in an increased reflection and a high insertion loss at high frequency, as shown Fig. 1. To broaden the absorption band to lower frequency and meanwhile maintain the high in-band transmission at high frequency, we can use more MR structures in a longer resistive element, and limit the length of each section between two adjacent MRs less than 0.3 λ_h.

A long resistive element can be constructed by cascading two MR structures with three short sections. Fig. 4 shows a unit cell of FSR with broadband absorption by placing this long resistive element with two MRs upon a bandpass FSS. The element of the bandpass FSS is a slot-type four-legged loaded element [1] with the periodicity of 9 mm × 9 mm.

An absorber can be constructed by replacing the bandpass FSS with a PEC plane to verify its broadened absorption. Its absorption performance is simulated by CST, together with that of an absorber structure with only one MR in the resistive element, as shown in Fig. 5. The two absorber structures have the same thickness of 14 mm. It can be seen that the absorption band of the absorber with short resistive element is from 3.2 GHz to 8.4 GHz, while the absorption bandwidth of the absorber with long resistive element is broadened to be 2.4–8.6 GHz, with the fractional bandwidth of 112%. The absorptive performance at low frequency below 3 GHz is improved. Besides, both the two absorber structures are nearly total-reflected around 10 GHz, because their resistive elements are nearly transparent at the resonance frequency of the MR.

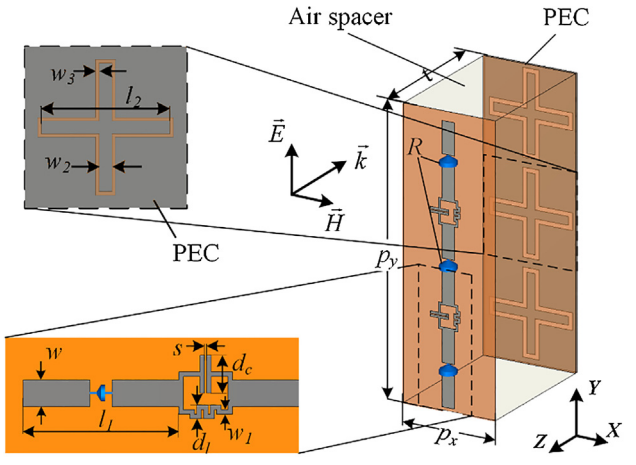

Fig. 4. Unit cell of single-polarized FSR with broadband absorption (physical dimensions: p_x = 9 mm, p_y = 27 mm, t = 14 mm, l_1 = 7 mm, l_2 = 7.2 mm, d_c = 1.5 mm, s = 0.1 mm, d_l = 0.4 mm, w = 1 mm, w_1 = 0.1 mm, w_2 = 0.2 mm, w_3 = 1.2 mm; lumped element: R = 210 Ω).

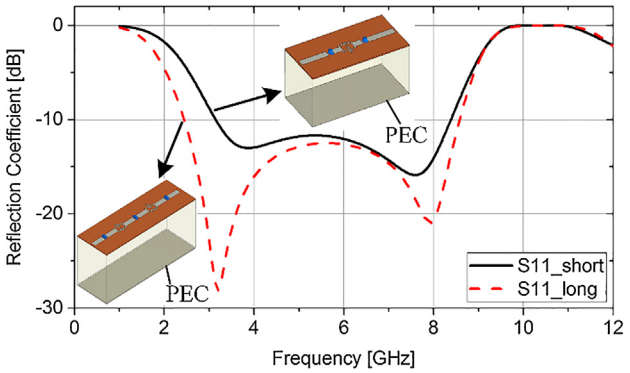

Fig. 5. Reflection coefficients of the absorbers with a short resistive element (single MR) and a long resistive element (two MRs).

For the FSR depicted in Fig. 4, the bandpass FSS should not only operate at the resonance frequency of MR to guarantee the transmissive performance, but also become total-reflected at low frequency and perform as the ground plane to obtain the broadband absorption. The frequency responses of the bandpass FSS under TE- and TM-polarized oblique incidence is shown in Fig. 6. As the incident angle increases, the transmission band of the bandpass FSS is at a steady frequency of 10 GHz under both the TE- and TM-polarized incidences. Besides, it is nearly total-reflected over 0–8 GHz, where it performs as the ground plane for the resistive sheet to realized broadband absorption.

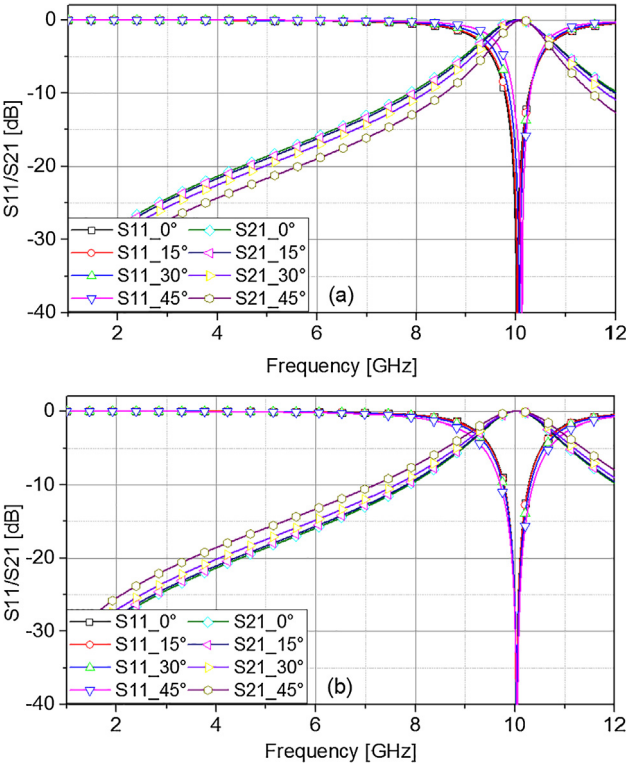

Fig. 6. Reflection/transmission coefficients of the bandpass FSS under oblique incidence (a) TE; (b) TM.

Fig. 7 shows the frequency response of the single-polarized FSR under TE-polarized oblique incidence. The absorption band with reflection coefficient less than −10 dB is from 2.4 GHz to 8 GHz and the transmission band locates at 9.7 GHz with insertion loss less than 0.4 dB. Due to the mutual coupling between the resistive sheet and the bandpass FSS, the transmission band is slightly shifted to 9.7 GHz. The absorption bandwidth becomes wider as the incident angle increases to 30°, but the reflection coefficient around 6 GHz increases to −7 dB under 45° incidence. The transmission band stabilizes at 9.7 GHz with insertion loss less than 0.5 dB in all the simulated scenarios.

3. Polarization-independent FSR

In the former section, a single-polarized FSR with a broadened absorption band at low frequency and a transmission band at high frequency is designed, but it is only capable of handling one polarization. We notice that the linear resistive element is of very small dimension in x-direction (only 2.4 mm), which is less than 0.1 λ at the whole simulated band 1–12 GHz. It can be concluded based in Fig. 1 that an x-polarized incident wave can totally pass through the resistive element at the whole band. This provides an inspiration to design polarization-independent FSR by placing two arrays of such linear resistive elements, orthogonal to each other.

A unit cell of the polarization-independent FSR is depicted in Fig. 8. The resistive sheet is a dual-layer structure printed on a dielectric substrate with thickness of 0.25 mm and $\varepsilon_r = 2.65$. Two identical and orthogonal arrays of resistive elements are printed on different sides of the dielectric substrate. Each resistive element is realized by cascading three short sections using two MR structures. Each short section is with the length of $0.25\lambda_h$ and loaded with a lumped resistor in the center. The two MR structures are of the same dimensions to resonate at the same frequency. The resistive element and the bandpass FSS is of the same dimensions with the single-polarized FSR in Fig. 4.

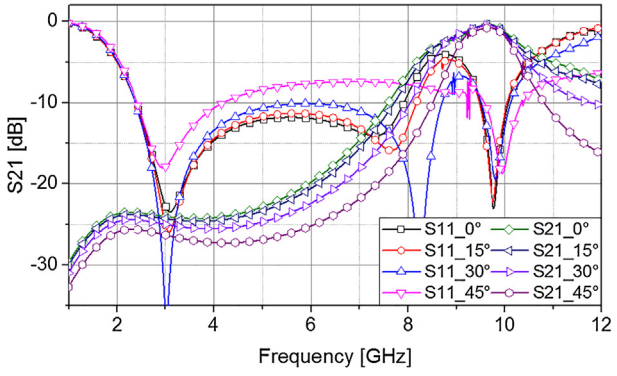

Fig. 7. Reflection/transmission coefficients of the single-polarized FSR under TE-polarized oblique incidence.

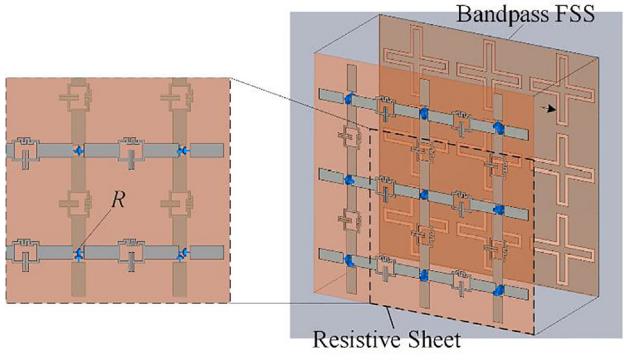

Fig. 8. Unit cell of the polarization-independent FSR.

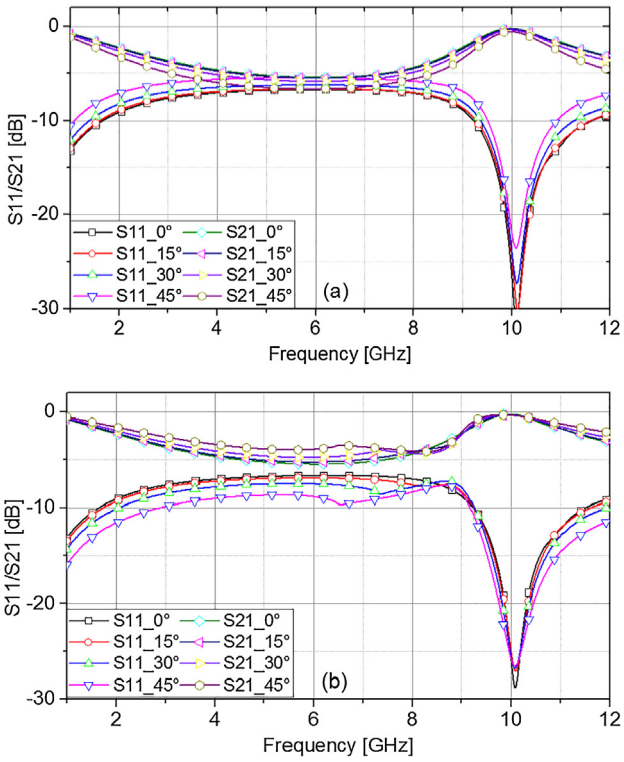

Fig. 9. Reflection/transmission coefficients of the polarization-independent resistive element at (a) TE- and (b) TM-polarized incidence.

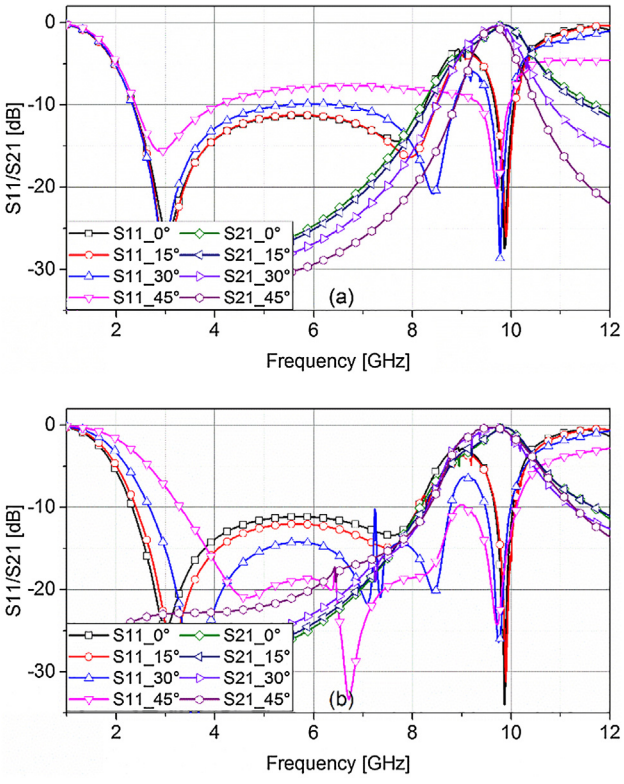

Fig. 10. Reflection/transmission coefficients of the polarization-independent FSR at (a) TE- and (b) TM-polarized incidences.

For an x-/y-polarized incident wave, only the array of resistive elements parallel with the E-field direction can be induced by the incident wave, while the other array doesn't work. The simulated reflection and transmission coefficients of the polarization-independent resistive sheet under both TE- and TM-polarized oblique incidences are shown in Fig. 9. A transmission band with the insertion loss less than 0.3 dB is obtained at 10 GHz in all the simulated scenarios. Since the MR structure is of very small dimensions, it can be regarded as a quasi-lumped circuit, so that the polarizations and incident angles have little effect on the transmission band. It resonates to be infinite impedance around 10 GHz and separates the long metallic dipole into three short section in the view of induced current. The incident wave can pass through this resistive sheet with very low insertion loss.

The absorptive/transmissive performance of the polarization-independent FSR is shown in Fig. 10. The results under TE-polarized incidences are almost the same to that of the single-polarized FSR as shown in Fig. 7. Under TM-polarized incidences, as the incident angle increases, the absorption bandwidth decreases but the absorption rate increases. The insertion loss at 9.7 GHz is lower than 0.5 dB in all the simulated scenarios. In conclusion, the absorptive/transmissive performance of the FSR structure is polarization-independent.

4. Experiment and discussion

To verify the polarization-independent absorptive/transmissive performance of the FSR, a prototype was fabricated and measured. A photo of the prototype is shown in Fig. 11. Both the resistive sheet and the bandpass FSS were printed on F_4BM dielectric substrates with thickness of 0.25 mm and permittivity of 2.65. Chip resistors were welded into the resistive sheet. The resistive sheet and the bandpass FSS were fixed in different surfaces of a Polymethacrylimide (PMI) foam spacer ($\varepsilon_r \approx 1$) with thickness of 14 mm using nylon screws.

The absorptive/transmissive performance of this prototype was measured in an anechoic chamber. The measured and simulated reflection and transmission coefficients under different polarizations and incidence angles are shown in Fig. 12. For oblique incidences under both TE- and TM-polarizations, the measured absorption band covers the band from 3 GHz to 8 GHz, which is little worse than the simulated results. The measured transmission band is shifted to 10.2 GHz with insertion loss less than 0.5 dB. The discrepancy between the measured and simulated results is mainly caused by fabrication and measurement errors.

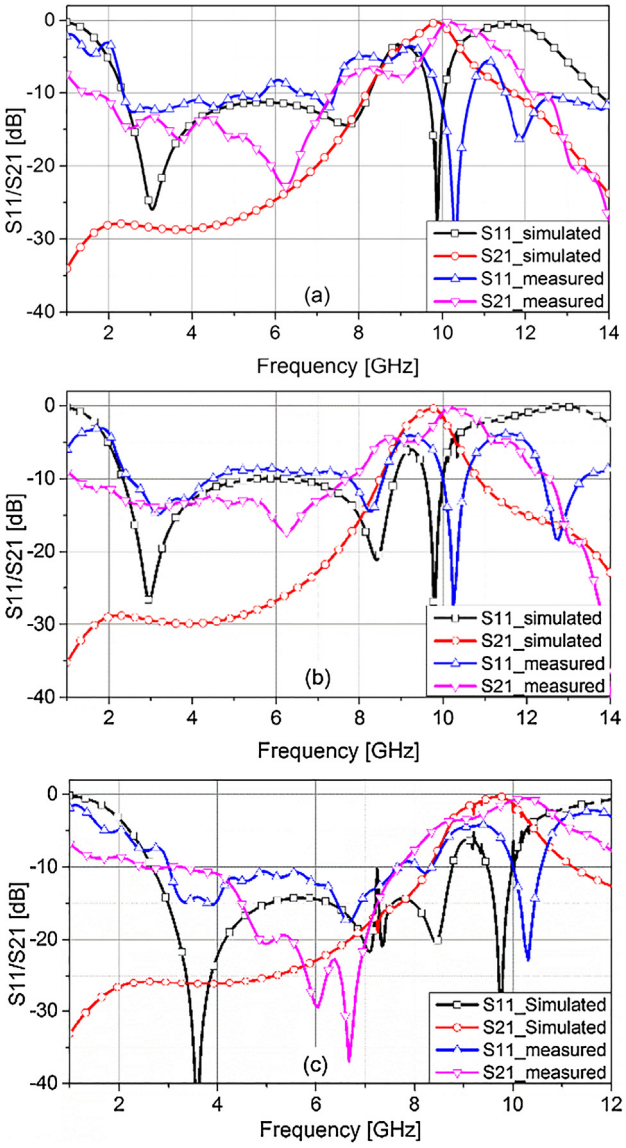

Fig. 12. Simulated and measured reflection/transmission coefficients of the polarization-independent FSR at (a) normal incidence; (b) TE_30°; (c) TM_30°.

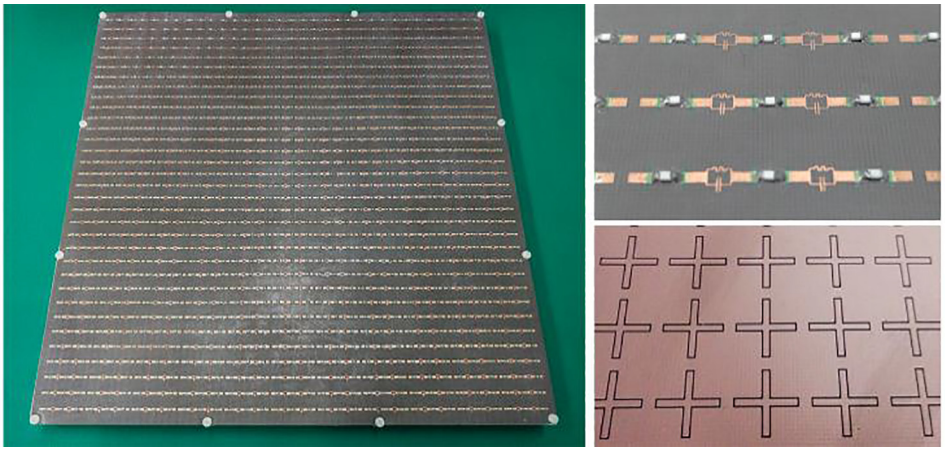

Fig. 11. Prototype of the FSR.

Table 1
Performance comparison of FSR designs.

Ref.	Polarization	Absorption band (fractional bandwidth)	Transmission band/insertion loss
[8]	Dual	10–18 GHz (57%)	4.6 GHz/0.3 dB
[9]	Dual	3–9 GHz (100%)	1 GHz/1 dB
[10]	Single	4.8–9.3 GHz (63.8%)	4.15 GHz/2.4 dB
[11]	Dual	3–9 GHz (100%)	1 GHz/0.3 dB
[12]	Dual	3–9 GHz (100%)	10 GHz/0.2 dB
[13]	Dual	5.5–13 GHz (81%)	21 GHz/1.2 dB
[14]	Single	2.8–8.3 GHz (99.1%)	9.7 GHz/0.5 dB
[15]	Single	2.7–8.3 GHz (101.8%)	9.45 GHz/1.5 dB
[16]	Dual	2.83–8.51 GHz (100%)	4.66 GHz/0.36 dB
[17]	Dual	0.92–1.43 GHz (43.2%) 2.84–3.31 GHz (15.3%)	2.2 GHz/0.5 dB
[18]	Dual	1.9–5.1 GHz (91.4%) 7.1–9.8 GHz (31.9%)	6.3 GHz/0.6 dB
[19]	Dual	1.79–2.6 GHz (43.9%) 4.5–5.25 GHz (15.4%)	3.68 GHz/1.28 dB
[20]	Single	1.7–2.19 GHz (25%) 3.95–8.64 GHz (37.2%)	2.93 GHz/0.73 dB
[21]	Dual	1.3–6 GHz (128%) 9.5–12.5 GHz (27.3%)	8.2 GHz/1.5 dB
[22]	Dual	3.76–8.7 GHz (79.3%) 12–16.08 GHz (29%)	10.3 GHz/0.3 dB
This work	Dual	2.35–8.25 GHz (111.3%)	9.8 GHz/0.4 dB

To evaluate the absorptive/transmissive performance of the FSR in this work, we list the polarization as well as the absorptive/-transmissive performances of several FSR designs in previous publications in Table 1. The FSR designs in [8–11] only have a transmission band below the absorption band. The designs in [12–15] can achieve a transmission band above the absorption band. The works in [16–22] have a transmission band within two absorption bands. Compared to these works, the design in this paper possesses a lower insertion loss at the transmission band and a wider absorption bandwidth at low frequency. Besides, the polarization-independent absorptive/transmissive performance is of great practical merit.

5. Conclusion

A polarization-independent FSR with broadband absorption at low frequency and high in-band transmission at high frequency has been designed and assessed in this study. It is composed of a MR-based resistive sheet and a bandpass FSS. To obtain a transmission band with low insertion loss, both the resistive sheet and the bandpass FSS should be nearly transparent at high frequency. By inserting MR structures into a resistor-loaded metallic dipole element, the induced current distribution on the resistive element at different frequencies can be controlled as expected. On this basis, a broadening of absorption band to lower frequency is realized by cascading three resistor-loaded metallic dipole elements with two same MR structures. Besides, extension to arbitrary polarizations is achieved by simply printing two aforesaid resistive elements orthogonal to each other on different surfaces of a dielectric substrate. The insertion loss is lower than 0.4 dB at 9.7 GHz under oblique incidence up to 45°, and the −10 dB absorption bandwidth spans from 2.35 GHz to 8.25 GHz under both TE-and TM-polarized incident waves.

Acknowledgments

This work was supported by the National Natural Science Foundation of China (Grant No. 61571448).

Appendix A. Supplementary material

Supplementary data to this article can be found online at https://doi.org/10.1016/j.aeue.2018.09.013.

References

[1] Munk BA. Frequency Selective Surfaces: Theory and Design. New York: Wiley; 2000.
[2] Kim PC, Lee DG, Seo IS, Kim GH. Low-observable radomes composed of composite sandwich constructions and frequency selective surfaces. Compos Sci Technol 2008;68(9):2163–70.
[3] Costa F, Monorchio A, Manara G. Analysis and design of ultra-thin electromagnetic absorbers comprising resistively loaded high impedance surfaces. IEEE Trans Antennas Propag. 2010;58:1511–58.
[4] Sun L, Cheng H, Zhou Y, Wang J. Design of a lightweight magnetic radar absorber embedded with resistive FSS. IEEE Antennas Wireless Propag Lett 2012;11:675–8.
[5] Zhou Y, Pang Y, Cheng H. Design and realization of a magnetic-type absorber with a broadened operating frequency band. Chin Phys B 2013;22:015201.
[6] Munk BA. Metamaterials: Critique and Alternatives. New Jersey: Wiley; 2009. p. 62–70.
[7] Motevasselian A, Jonsson BLG. Design of a wideband rasorber with a polarisation-sensitive transparent window. IET Microw Antennas Propag. 2011;6:747–55.
[8] Costa F, Monorchio A. A frequency selective radome with wideband absorbing properties. IEEE Trans Antennas Propag. 2012;60(6):2740–7.
[9] Liu L, Guo P, Huang J, Wu W, Mo J, Fu Y, et al. Design of an invisible radome by metamaterial absorbers loaded with lumped resistors. Chin Phys Lett 2012;29:012101.
[10] Li B, Shen Z. Wideband 3D frequency selective rasorber. IEEE Trans Antennas Propag 2014;62:6536–41.
[11] Chen Q, Bai J, Chen L, Fu Y. A miniaturized absorptive frequency selective surface. IEEE Antennas Wireless Propag Lett 2015;14:80–3.
[12] Chen Q, Yang S, Bai J, Fu Y. Design of absorptive/transmissive frequency-selective surface based on parallel resonance. IEEE Trans Antennas Propag 2017;65:4897–902.
[13] Chen X, Li Y, Fu Y, Yuan N. Design and analysis of lumped resistor loaded metamaterial absorber with transmission band. Opt Exp 2012;20:28347–52.
[14] Chen Q, Chen L, Bai JJ, Fu Y. Design of absorptive frequency selective surface with good transmission at high frequency. Electron Lett 2015;51:885–6.
[15] Chen Q, Liu L, Chen L, Bai J, Fu Y. Absorptive frequency selective surface using parallel LC resonance. Electron Lett 2016;52:418–9.
[16] Shang Y, Shen Z, Xiao S. Frequency-selective rasorber based on square-loop and cross-dipole arrays. IEEE Trans Antennas Propag 2014;62:5581–9.
[17] Shen Z, Wang J, Li B. 3-D frequency selective rasorber: concept, analysis, and design. IEEE Trans Microw Theory Techn 2016;64:3087–96.
[18] Huang H, Shen Z. Absorptive frequency-selective transmission structure with square-loop hybrid resonator. IEEE Antennas Wireless Propag Lett 2017;16:3212–5.
[19] Han Y, Che W, Xiu X, Yang W, Christopoulos C. Switchable low-profile broadband frequency-selective rasorber/absorber based on slot arrays. IEEE Trans Antennas Propag 2017;65:6998–7008.
[20] Yu Y, Shen Z, Deng T, Luo G. 3-D frequency-selective rasorber with wide upper absorption band. IEEE Trans Antennas Propag 2017;65:4363–7.
[21] Zhou Q, Liu P, Wang K, Liu H, Yu D. Absorptive frequency selective surface with switchable passband. AEU – Int J Electron Commun 2018;89:160–6.
[22] Chen Q, Sang D, Guo M, Fu Y. Frequency-selective rasorber with inter-absorption band transparent window and interdigital resonator. IEEE Trans Antennas Propag 2018;66:4105–14.